

Polarimetry of 600 pulsars from observations at 1.4 GHz with the Parkes radio telescope

Simon Johnston^{1*} and Matthew Kerr^{1,2}

¹CSIRO Astronomy and Space Science, Australia Telescope National Facility, PO Box 76, Epping, NSW 1710, Australia

²Space Science Division, Naval Research Laboratory, Washington, DC 20375-5352, USA

Accepted 29 November 2017. Received 29 November 2017; in original form 29 November 2017

ABSTRACT

Over the past 13 years, the Parkes radio telescope has observed a large number of pulsars using digital filterbank backends with high time and frequency resolution and the capability for Stokes recording. Here we use archival data to present polarimetry data at an observing frequency of 1.4 GHz for 600 pulsars with spin-periods ranging from 0.036 to 8.5 s. We comment briefly on some of the statistical implications from the data and highlight the differences between pulsars with high and low spin-down energy. The dataset, images and table of properties for all 600 pulsars are made available in a public data archive maintained by the CSIRO.

Key words: pulsars:general

1 INTRODUCTION

The first pulsar discovery was made nearly 50 years ago (Hewish et al. 1968) and it was quickly realised that pulsars were often highly polarized (Lyne & Smith 1968). One of the defining characteristics of pulsars is the long-term pulse profile stability combined with the complexity of the profiles in both total intensity and polarization. The polarimetry of pulsars leads to an understanding of the geometry of the star, an estimate of the height of the radio emission, clues as to the emission physics and the overall structure of the pulsar beam.

It became apparent that the radio emission is strongly tied to the magnetic field lines and the position angle of the linear polarization is determined by the angle of the magnetic field line as it sweeps past the line of sight (Komesaroff 1970). This in turn leads to an understanding of the geometry of the star, in particular the angle between the rotation and magnetic axes (α) can be estimated via the ‘rotating vector model’ (Radhakrishnan & Cooke 1969). Furthermore, relativistic effects can offset the position angle swing from the total intensity profile and this can be used to measure the height of the radio emission (Blaskiewicz et al. 1991). The total intensity profiles themselves are used to infer the structure of the emission beam, with Rankin (1990, 1993) favouring a structured model with ‘core’ and ‘cone’ emission whereas Lyne & Manchester (1988) prefer a more patchy, random emission beam. Traditionally it was thought that lower frequencies arise from

higher in the magnetosphere than higher frequencies (see e.g. Cordes 1978) but more recent evidence suggests that emission arises over a wide range of heights in a given pulsar at a single frequency (Gupta & Gangadhara 2003; Karastergiou & Johnston 2007).

The position angle swing as a function of pulse phase is often interrupted by jumps of 90° and this led to the idea that emission was present in two orthogonal modes (Ekers & Moffet 1969; Backer et al. 1976). Whether the modes are disjoint or superimposed has been debated by observers (McKinnon & Stinebring 1998; Edwards & Stappers 2004) and theorists alike (Gil et al. 1991; Melrose et al. 2006; van Straten & Tiburzi 2017) and the question remains unresolved.

Finally the origin of the polarization remains unclear with circular polarization discussed empirically and theoretically by e.g. Radhakrishnan & Rankin (1990) and Melrose & Luo (2004). Refraction and propagation effects in the magnetosphere and conversion between the modes in a ‘polarization limiting region’ has been put forward by e.g. Petrova & Lyubarskii (2000) and Petrova (2006) as an explanation for features seen in linear polarization. Cyclotron absorption in the pulsar magnetosphere (Blandford & Scharlemann 1976) may play a role in both the profile shape and the polarization characteristics. Luo & Melrose (2001) show that the trailing part of profiles are suppressed relative to the leading part and discuss the possibility that one of the polarized modes may also be absorbed, preventing mode mixing and leading to a high degree of polarization in the profile as a whole.

Publication of polarimetry for a large sample of pulsars

* email: Simon.Johnston@csiro.au

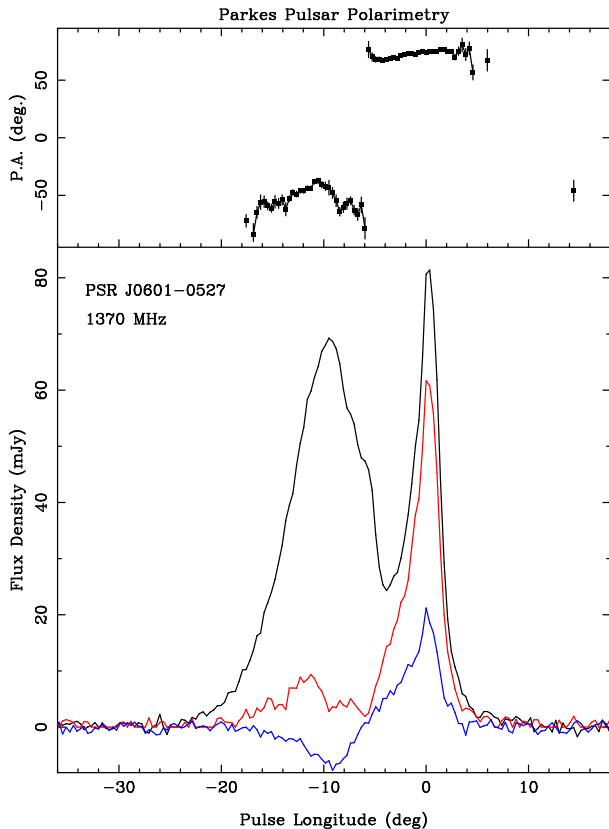


Figure 1. PSR J0601–0527 in full polarization. In the lower panel the black line denotes Stokes I, the red trace shows the linear polarization and the blue trace the circular polarization. Left-hand circular polarization is defined to be positive. The top panel shows the position angle of the linear polarization, corrected to infinite frequency using the RM listed in the table. Position angles are only plotted when the linear polarization exceeds 3 sigma. The zero point of pulse longitude is set to the peak of the total intensity profile.

is therefore vital for tackling the problems outlined above. Observations made at 1.4 GHz have been published for 300 pulsars with the Lovell telescope in the UK (Gould & Lyne 1998), 98 pulsars with the Arecibo telescope in the USA (Weisberg et al. 1999) and 66 pulsars with the Parkes telescope in Australia (Manchester et al. 1998). Recent polarimetric observations at lower frequencies include those compiled by Hankins & Rankin (2010) and Mitra et al. (2016). Here, we provide data on 600 mostly southern hemisphere pulsars observed with the Parkes radio telescope over the past decade. The aim of this paper is threefold. First to make available the entire dataset of southern hemisphere pulsars, flux and polarimetrically calibrated, in PSRFITS format (Hotan et al. 2004) for use by other researchers. Secondly, to provide thumb-nail images for all the pulsars and finally to provide in tabular form the polarization characteristics for this large sample of pulsars.

In Section 2 we outline the observations, section 3 deals with the data reduction, section 4 presents the results and section 5 briefly discusses the implications in general terms. Section 6 informs readers of how to access the data.

Table 1. Origin of the archival pulsar observations

ID	PI	Obs Dates	Rx	Pulsars	Ref
P574	Johnston	2008-2017	MB	301	1
P535	Johnston	2006-2007	H-OH	149	
P236	Han	2006-2007	MB	54	2
P630	Johnston	2009-2012	MB	48	3
P439	Johnston	2004-2005	H-OH	21	4
P875	Jankowski	2014	MB	21	5
Misc				6	

1. Johnston & Weisberg (2006); Weltevrede & Johnston (2008); Weltevrede et al. (2010); Abdo et al. (2013); Rookyard et al. (2015a). 2. Profiles unpublished, data presented in Han et al. (2017). 3. Tiburzi et al. (2013). 4. Johnston et al. (2005, 2007). 5. Profiles unpublished, data presented in Jankowski et al. (2017).

2 OBSERVATIONS

The Parkes radio telescope is a 64-m dish located near Parkes, NSW, Australia. Functional since 1963, the telescope has had a long history of observations of radio pulsars since their discovery in 1967. In 2004, the telescope acquired digital backend systems to replace the aging analogue spectrometers. These Digital Filterbanks (DFBs) were FPGA-based correlators, capable of recording full Stokes information over a large number of frequency channels. During pulsar observations, the data are folded modulo the pulsar’s topocentric spin frequency to form a ‘sub-integration’ of typical duration 10–30 s. These sub-integrations are combined until the desired total observing length had been reached.

At observing frequencies near 1.4 GHz two main receivers have been available over the past decade, the multi-beam receiver (Staveley-Smith et al. 1996) and the H-OH receiver (Thomas et al. 1990). For the purposes described here, both receivers are generally used over 256 MHz of bandwidth from 1240 to 1496 MHz. Typically the bandwidth is divided into 512 or 1024 frequency channels each of width 0.25 or 0.5 MHz. For both systems, it is possible to inject a square-wave signal of known periodicity directly into the feed for calibration purposes. For further details of the receiver and backend systems see Manchester et al. (2013).

In this paper we concentrate on ‘normal’ pulsars with spin periods greater than 30 ms and which are not considered to have been recycled. For a systematic view of the polarimetry of millisecond pulsars in the southern hemisphere see Dai et al. (2015). The most recent publication of a systematic survey of southern pulsars in polarization dates back nearly two decades (Manchester et al. 1998) and have poorer time and frequency resolution than the data collected here.

The observations span a time period from 2004 November to 2017 February and data were taken from the public Data Archive Portal (Hobbs et al. 2011; <http://data.csiro.au>). A total of 600 pulsars were used for this work, many of them observed multiple times. Table 1 shows the origin of the data, listing the project identifier (ID) and principal investigator (PI), the dates of the observations, the receiver used (Rx; MB denotes the multi-beam receiver), the number of pulsars and a reference to previously published material.

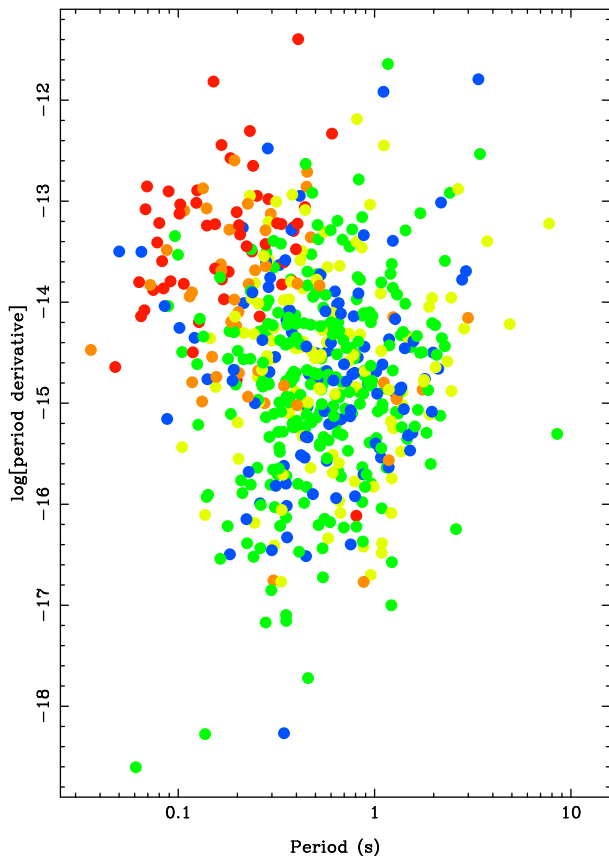


Figure 2. The period-period derivative plane for 594 pulsars. The colour represents the fraction of linear polarization with red the highest and blue the lowest.

3 DATA REDUCTION

The entire dataset under consideration here has been reprocessed for this paper. We outline the basic steps below.

3.1 Phase and gain calibration

A calibrator observation consists of pointing the telescope at a patch of blank sky and injecting a square-wave with a 50% duty cycle and known periodicity directly into the feed. The equivalent flux density of the calibrator is ~ 1 Jy. A calibrator observation is first located as close in time and in sky location as possible to the pulsar observation. For the vast majority of observations, the calibrator was observed within one hour of the pulsar observation and in the same area of sky. Frequency channels which are corrupted (either edge channels or channels with interference) are identified and deleted from the data. Then, the relative gain between the two linear polarization probes are determined along with the phase offset between them on a channel-by-channel basis.

3.2 Flux density calibration

Flux density calibration is carried out on a regular basis using the source Hydra A as a reference. Hydra A has a flux density of 43.1 Jy at 1.4 GHz. For the majority of the observations described here, flux density calibration measure-

ments were made within two weeks of the pulsar observations. Results from the flux density calibration are applied to the pulsar data on a per-channel basis to convert from digitiser counts into units of Jy.

3.3 Receiver characterisation

The multibeam receiver shows a modest level of cross-polarization and/or non-orthogonality. We characterize this following the method of van Straten (2004) where long observations, over a range of parallactic angles, of a highly polarized source (typically PSR J0437–4715) are used to model the receiver response. Such observations are carried out every few months. We compute and apply the resulting calibration solutions with the PSRCHIVE routine PCM. For the H-OH receiver, each pulsar was observed at least twice with the feed rotated by 90° between observations to minimise the impact of the already small impurities in the receiver (see details in Johnston et al. 2005).

3.4 Pulsar data reduction

The pulsar data are first corrected for gain and phase by applying the solutions obtained from the calibrator and then converted to Jy by applying the flux calibration solution. Note that any corrupt frequency channels identified in the previous step are also then flagged in the pulsar data. Receiver calibration solutions are then applied. Next, the pulsar observation is examined, and corrupt sub-integrations are flagged and removed from the data. Finally, the pulsar data is averaged in both time and frequency, taking into account the rotation measure (RM) and dispersion measure (DM) of the pulsar. The majority of the RM values were obtained from the large samples reported in Han et al. (2006), Noutsos et al. (2008) and Han et al. (2017). Several observations of the same pulsar may be available. If so, the (flux and polarimetrically calibrated) observations are added together after alignment via cross-correlation. The final output contains a Stokes I,Q,U,V datastream covering the pulsar period with a resolution of 1024 or 512 time samples.

3.5 Polarization conventions

The polarization data have absolute calibration using the conventions outlined in van Straten et al. (2010). Position angles are defined as increasing counter-clockwise on the sky (see Everett & Weisberg 2001). Circular polarization in pulsar astronomy uses the IEEE convention for left-hand and right-hand, a convention which differs from the one adopted by the IAU and which most radio interferometers apply. In the data presented here, left-hand circular polarization is positive as per the IEEE and pulsar convention. A sample pulsar is shown in Figure 1.

4 RESULTS

The distribution of 594 pulsars on the period-period derivative ($P - \dot{P}$) diagram is shown in Figure 2 (6 pulsars have no measured \dot{P}). The periods range from 35 ms to 8.5 s and there is 7 orders of magnitude coverage in \dot{P} .

Table 2 lists the polarization properties of the first 25

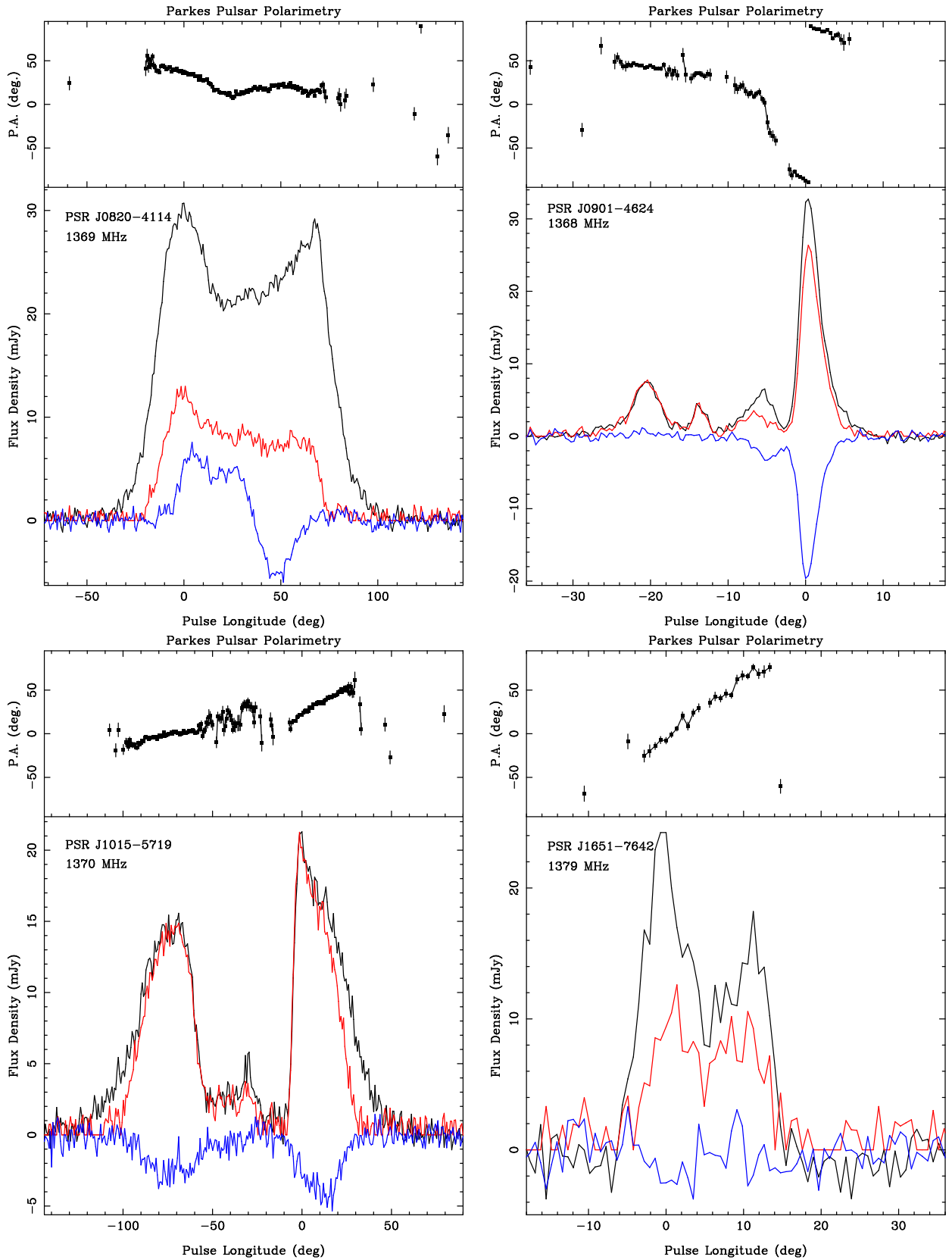


Figure 3. Example pulsars from the discussion. Top left is PSR J0820-4114 an example of a low \dot{E} pulsar with a large width, top right is PSR J0901-4624 which has a large fractional circular polarization. Bottom left is an example of a wide-double, high \dot{E} pulsar PSR J1015-5719 and bottom right shows a rare example of a pulsar with high linear fraction in spite of low \dot{E} . See also the caption to Figure 1.

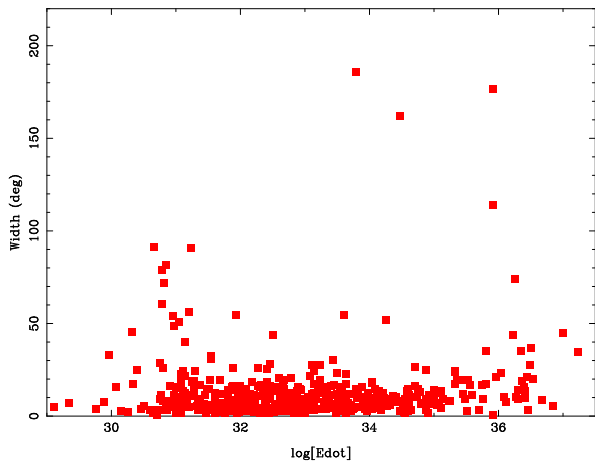


Figure 4. Spin-down energy (\dot{E}) versus pulse width (W_{50}) for 501 pulsars.

pulsars (the full table is available through the on-line material). The table shows the pulsar parameters, spin period (P), dispersion measure (DM) and the spin-down energy (\dot{E}) given by

$$\dot{E} = 4\pi^2 I \dot{P} P^{-3} \quad (1)$$

where I is the moment of inertia of the star (taken to be 10^{45} g cm²). The rotation measure (RM) as used in the data reduction is listed. The table then lists then number of bins (nbin) across the pulsar profile and the off-pulse (i.e. the noise) root-mean-square (σ_I) in mJy per bin. The flux density at 1.4 GHz ($S_{1.4}$) is listed along with the width of the profile (in degrees) at 50% of the peak (W_{50}). Taking into account systematic effects in the calibration, we estimate the error on $S_{1.4}$ to be 10%. The error on W_{50} is $\lesssim 0.5^\circ$ when the signal to noise ratio is high, but quickly becomes large once the signal to noise ratio drops below 10. Finally, the percentage of linear polarization (L/I), of circular polarization (V/I), and of the absolute value of the circular polarization ($|V|/I$) is given along with the error bar. For computation of the fractional linear polarization we follow Everett & Weisberg (2001), in particular their Equation 11 is used to debias L . In order to compute the $|V|/I$ we have followed the prescription given in Karastergiou & Johnston (2004) which ensures that the off-pulse baseline retains a mean of zero. The error bar is given by the quadrature sum of the formal fits to the profile, taking into account σ_I , and our estimate of the systematic errors (3%).

The last column contains a flag. “W” implies the pulsar has a peak flux density less than 15 times the rms; W_{50} and the fractional polarization values should be treated with caution. There are 69 such pulsars in the sample. “R” denotes a pulsar for which we could obtain no RM either because the pulsar is weak or the fractional linear polarization is intrinsically low. The RM is set to zero for these cases. A total of 55 pulsars fall into this category (of which 25 are also classified as “W”). “S” denotes a pulsar showing strong (clearly visible by eye) scatter-broadening of the profile due to the interstellar medium. In this case, the true pulse width will be smaller than the measured width and the measured fractional polarization will be lower than the true value. There are 32 pulsars with this flag. “N” denotes pulsars that are

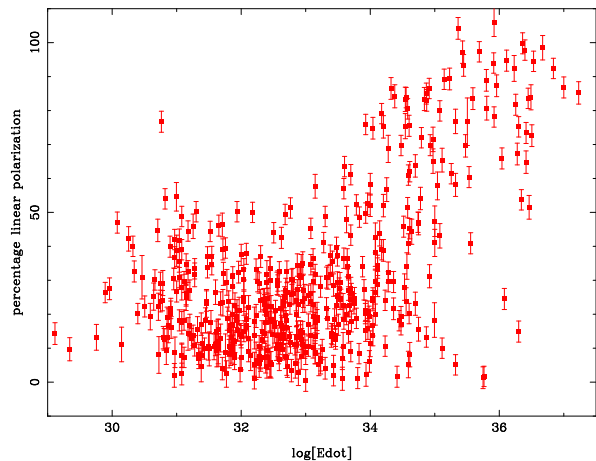


Figure 5. Spin-down energy (\dot{E}) versus percentage linear polarization for 501 pulsars.

not flux calibrated. There are 14 pulsars in this category; their flux densities have been set to zero in the table. “I” denotes the 20 pulsars with an interpulse.

5 DISCUSSION

In the discussion that follows, pulsars with a “W” or “S” flag have been excluded from the analysis and the figures. Sample pulsars which form part of the discussion can be found in Figure 3.

Figure 4 shows W_{50} against \dot{E} . There are four groupings which stand out in the figure. First, the bulk of the pulsar population have $W_{50} \lesssim 25^\circ$; a slight rise in W_{50} to higher values of \dot{E} can be seen. Secondly there are a group of pulsars with $\dot{E} < 10^{32}$ erg s⁻¹ and $W_{50} \gtrsim 50^\circ$. These pulsars have small values of α , examples include PSRs J0820–4114 (see Figure 3), J1034–3224 and J1133–625. Thirdly there are the moderate \dot{E} pulsars with very large W_{50} . These are the interpulse pulsars such as PSR J0908–4913 (Kramer & Johnston 2008; Keith et al. 2010) where α is close to 90° and both poles are seen. Finally, some high \dot{E} pulsars have large widths. These are the “wide-doubles” identified by Johnston & Weisberg (2006) examples of which include PSRs J1015–5917 (see Figure 3) and J1302–6350. The geometry of these pulsars and the implications thereof have been examined in detail by Rookyard et al. (2015b).

Figure 5 shows \dot{E} versus linear polarization fraction and contains the striking result obtained by Weltevrede & Johnston (2008). Below \dot{E} of 10^{33} erg s⁻¹, only 3 objects have a linear fraction in excess of 55%, PSRs J0108–1431, J1651–7642 and J1805–1504 (see Figure 3). In contrast, above \dot{E} of $10^{35.5}$ erg s⁻¹ only 5 objects have $L/I < 50\%$, PSRs J1055–6028, J1413–6141, J1646–4346, J1833–0827 and J1837–0653. Figure 2 gives another representation of this effect. Pulsars at the top left of the diagram are highly polarized (red colour) as opposed to the remainder of the pulsars which have lower polarization (green/blue colours).

Figure 6 also shows some differences in the fractional circular polarization between the high \dot{E} and the low \dot{E} pulsars, with the high \dot{E} pulsars having a larger spread in circular polarization and a higher average. There is no preference

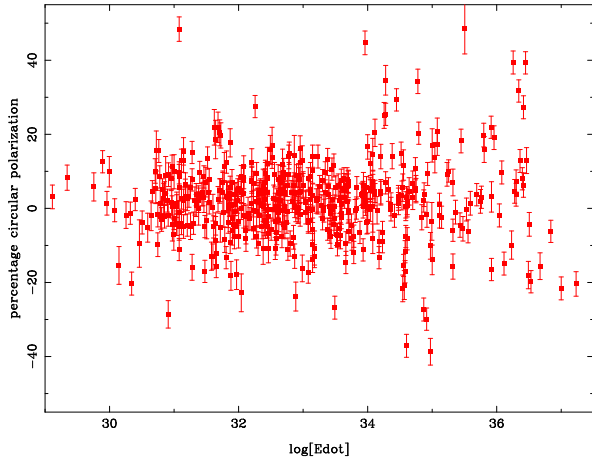


Figure 6. Spin-down energy (\dot{E}) versus percentage circular polarization for 501 pulsars.

for right or left handed circular. Only very few pulsars have $V/I \gtrsim 40\%$, examples are PSRs J0901–4624 (see Figure 3), J1410–7404 and J1915+1009, and there are no convincing examples of pulsars with $V > L$.

Figure 7 shows the relationship between P and W_{50} . Although there is a large scatter, generally pulsars with shorter periods have larger W_{50} . A straight line fit to these data has a slope of -0.29 and a width at a period of 1 s of 4.7° . This is generally consistent with results already in the literature (Rankin 1993; Kramer et al. 1998; Mitra & Rankin 2002; Weltevrede & Johnston 2008). All other things being equal, a slope of 0 would imply that the emission height is a fixed fraction of the light-cylinder radius whereas a slope of -0.5 implies a fixed emission height in km (see e.g. the discussion in Mitra & Rankin 2002). There are, however, many additional factors which muddy the interpretation of Figure 7. These include evolution of α with time (Tauris & Manchester 1998; Johnston & Karastergiou 2017), the patchiness of the beam (Lyne & Manchester 1988), the possibility of varying emission height as a function of period or age (Karastergiou & Johnston 2007), and the variation of emission height as a function of longitude (Gupta & Gangadhara 2003; Mitra & Rankin 2002).

The symmetry of pulsar profiles can also be examined. In Weltevrede & Johnston (2008) it was shown that there was a strong correlation between a pulsar’s profile and its time-reversed profile. Here we examine the relationship between the peak of the total intensity profile and its midpoint. The midpoint is defined as the half-way point between where the intensity of the leading edge of the profile first exceeds 50% of the maximum and where the intensity of the trailing edge first drops below 50% of the maximum. Figure 8 shows the offset between the location of the profile peak and its midpoint as a function of \dot{E} for 484 pulsars. In almost half (237/484) of the pulsars the profile peak coincides with the midpoint to within $\pm 1^\circ$. The remaining pulsars are split evenly between positive (peak lagging the midpoint) and negative values although at high \dot{E} a preponderance of negative values are seen indicating the peak on the trailing part of the profile (as also pointed out by Johnston & Weisberg 2006). This appears contrary to the cyclotron absorption ideas of Luo & Melrose (2001) but in

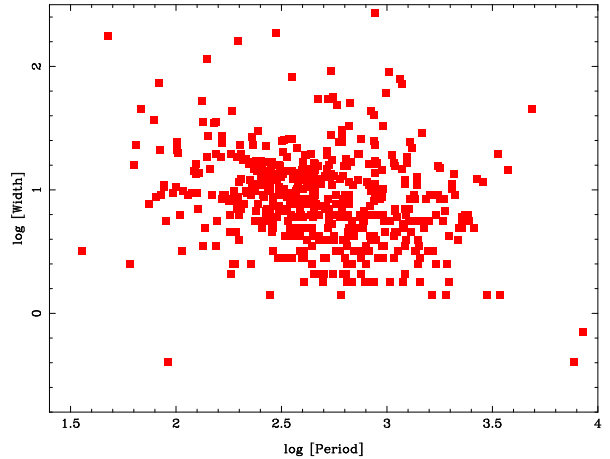


Figure 7. Log of the spin period (P) versus log of the pulse width (W_{50}) for 501 pulsars.

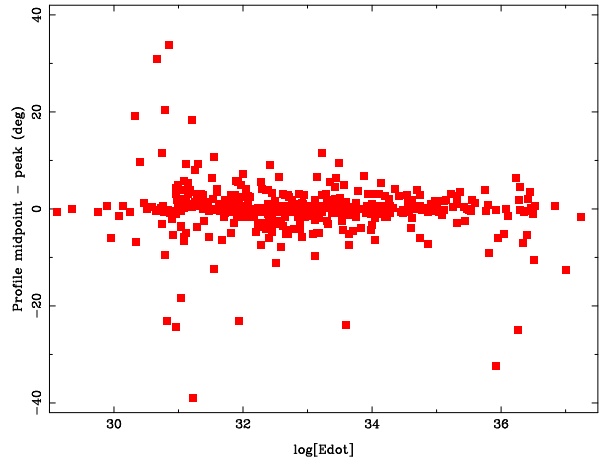


Figure 8. Spin-down energy (\dot{E}) versus symmetry offset for 484 pulsars.

line with the more complete treatment given in Fussell et al. (2003). Two examples of pulsars with asymmetric profiles are given in Figure 9. Both appear to be partial cones in the nomenclature of Lyne & Manchester (1988) and there is little evolution of the profile with observing frequency in either case. In PSR J0907–5157 we likely observe the trailing inner and outer cones with the leading outer cone not visible whereas for PSR J1047–6709 only the leading cone is detectable.

6 DATA ACCESS

The following data products are provided via the CSIRO’s Data Access Portal.

- A README file which describes the table columns, the figure caption and the paper reference.
- A single PSRFITS file for each of the 600 pulsars with either 512 or 1024 bins across the profile. These files can be manipulated with the PSRCHIVE package available via SOURCEFORGE. Both the PSRFITS format and PSRCHIVE are described in Hotan et al. (2004). The naming convention for the files is pulsarname.1400MHz.psrfits.

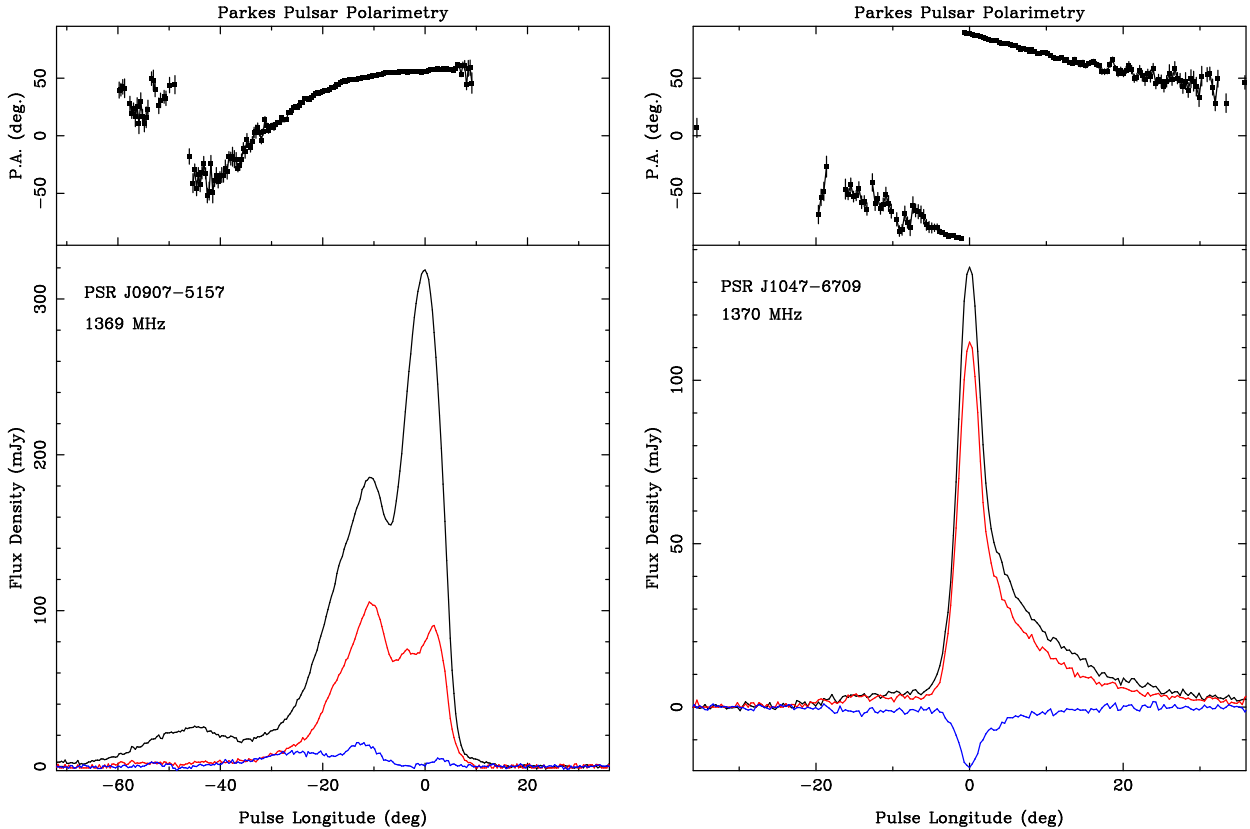


Figure 9. Two examples of asymmetric profiles. Left panel is PSR J0907-5157, heavily weighted towards the trailing edge, right panel is PSR J1047-6709 showing the profile dominates on the leading edge. See also the caption to Figure 1.

- A single figure in PNG format for each of the 600 pulsars similar to those shown in Figures 1 and 3. The naming convention is pulsarname.1400MHz.png.
- A table of 600 lines (one per pulsar) with the columns as in Table 2 but in csv format with the columns separated by commas.

The data can be accessed through the main portal entry at <http://data.csiro.au> and then searching on “pulsar polarimetry” or the data can be accessed directly via the published DOI <http://doi.org/10.4225/08/59952c840ae35>.

7 SUMMARY

In this paper we provide the polarization characteristics for 600 pulsars from observations taken at 1.4 GHz using the Parkes radio telescope since 2004. We have highlighted some of the statistical properties of the data, including differences between pulsars with high and low values of \dot{E} . All the data and the table of parameters are made available via public archive. A large fraction of these pulsars have also been observed at 0.7 and 3.1 GHz; future plans include a release of these data and a full multi-frequency comparison of the population.

ACKNOWLEDGMENTS

We thank G. Hobbs, A. Karastergiou, B. Koribalski and M. Kramer for useful discussions, C. Tiburzi for her datasets and R. Manchester for providing RMs prior to publication. L. Toomey provided valuable assistance with setting up the data archive. We thank the referee for a careful reading of the manuscript. The ATNF pulsar catalogue at <http://www.atnf.csiro.au/people/pulsar/psrcat/> was used for this work. The Parkes telescope is part of the Australia Telescope National Facility which is funded by the Commonwealth of Australia for operation as a National Facility managed by CSIRO. Work at NRL is supported by NASA.

REFERENCES

- Abdo A. A. et al., 2013, *ApJSS*, 208, 17
 Backer D. C., Rankin J. M., Campbell D. B., 1976, *Nat*, 263, 202
 Blandford R. D., Scharlemann E. T., 1976, *MNRAS*, 174, 59
 Blaskiewicz M., Cordes J. M., Wasserman I., 1991, *ApJ*, 370, 643
 Cordes J. M., 1978, *ApJ*, 222, 1006
 Dai S. et al., 2015, *MNRAS*, 449, 3223
 Edwards R. T., Stappers B. W., 2004, *A&A*, 421, 681
 Ekers R. D., Moffet A. T., 1969, *ApJ*, 158, L1
 Everett J. E., Weisberg J. M., 2001, *ApJ*, 553, 341
 Fussell D., Luo Q., Melrose D. B., 2003, *MNRAS*, 343, 1248
 Gil J. A., Snakowski J. K., Stinebring D. R., 1991, *A&A*, 242, 119
 Gould D. M., Lyne A. G., 1998, *MNRAS*, 301, 235
 Gupta Y., Gangadhara R. T., 2003, *ApJ*, 584, 418

Table 2. Pulsar polarization properties at 1.4 GHz (sample)

Jname	Period (ms)	DM (cm^{-3}pc)	RM (radm^{-2})	$\log(\dot{E})$ (ergs^{-1})	nbin	σ_I (mJy)	$S_{1.4}$ (mJy)	W_{50} (deg)	L/I %	V/I %	$ V /I$ %	err %	flag
J0034-0721	943.0	10.9	9.8	31.3	1024	0.27	11.12	14.4	10.7	7.7	7.5	3.0	
J0051+0423	354.7	13.9	-30.5	30.8	512	0.39	0.49	26.0	13.1	-2.3	11.2	3.3	
J0108-1431	807.6	2.4	-0.3	30.8	1024	0.57	1.37	11.6	76.7	15.5	13.1	3.1	
J0134-2937	137.0	21.8	13.0	33.1	1024	0.37	3.90	4.9	45.3	-17.2	16.9	3.0	
J0151-0635	1464.7	25.7	-7.0	30.7	512	1.01	1.57	28.8	29.1	-1.7	4.2	3.3	
J0152-1637	832.7	11.9	2.0	31.9	1024	0.44	2.14	6.3	15.1	1.1	6.0	3.0	
J0206-4028	630.6	12.9	-4.0	32.3	1024	0.51	0.75	2.8	10.6	9.3	9.9	3.1	
J0211-8159	1077.3	24.4	54.0	31.0	512	0.77	0.33	16.2	17.0	11.7	15.4	5.5	W
J0255-5304	447.7	15.9	32.0	31.1	1024	0.65	5.00	6.0	7.3	-4.1	5.5	3.0	
J0304+1932	1387.6	15.7	-8.3	31.3	1024	0.92	15.05	10.9	33.4	15.1	14.8	3.0	
J0343-3000	2597.0	20.2	33.7	29.1	1024	0.96	1.26	4.9	14.3	3.1	3.9	3.2	
J0401-7608	545.3	21.6	19.0	32.6	1024	0.42	3.80	13.4	28.6	-0.1	4.7	3.0	
J0448-2749	450.4	26.2	24.0	31.8	1024	1.01	2.04	8.4	23.9	-13.3	11.8	3.0	
J0450-1248	438.0	37.0	13.0	31.7	512	1.01	1.22	20.4	25.3	2.5	6.0	3.4	
J0452-1759	548.9	39.9	13.8	33.1	1024	0.47	16.83	17.6	18.9	3.6	4.2	3.0	
J0459-0210	1133.1	21.0	18.0	31.6	1024	1.50	0.63	3.2	10.4	-12.9	9.6	3.8	
J0520-2553	241.6	33.8	19.0	31.9	512	0.96	0.79	14.1	18.2	-4.3	5.0	3.6	
J0525+1115	354.4	79.4	37.0	31.8	1024	0.58	1.74	14.1	10.6	12.5	15.5	3.0	
J0528+2200	3745.5	50.9	-40.2	31.5	2048	2.48	8.90	14.6	36.9	-4.9	4.6	3.0	
J0533+0402	963.0	83.7	-71.2	30.9	1024	0.86	0.73	5.6	13.3	4.0	5.5	3.2	
J0536-7543	1245.9	17.5	25.2	31.1	1024	0.58	8.42	16.5	48.8	-11.1	11.0	3.0	
J0540-7125	1286.0	29.4	43.0	31.2	512	0.94	0.35	8.4	14.2	3.1	15.8	4.8	
J0543+2329	246.0	77.7	8.7	34.6	1024	0.53	12.90	7.7	45.2	-8.2	7.9	3.0	
J0601-0527	396.0	80.5	64.0	32.9	1024	0.62	2.59	14.4	30.9	4.4	11.3	3.0	
J0614+2229	335.0	96.9	69.0	34.8	1024	0.73	3.60	6.7	72.0	20.3	20.1	3.0	

Han J. L., Manchester R. N., Lyne A. G., Qiao G. J., van Straten W., 2006, *ApJ*, 642, 868
Han J. L., Manchester R. N., van Straten W., Demorest P., 2017, *ApJ* In Press
Hankins T. H., Rankin J. M., 2010, *AJ*, 139, 168
Hewish A., Bell S. J., Pilkington J. D. H., Scott P. F., Collins R. A., 1968, *Nat*, 217, 709
Hobbs G. et al., 2011, *Publ. Astron. Soc. Australia*, 28, 202
Hotan A. W., van Straten W., Manchester R. N., 2004, *PASA*, 21, 302
Jankowski F., van Straten W., Keane E. F., Bailes M., Barr E., Johnston S., Kerr M., 2017, *MNRAS* In Press.
Johnston S., Hobbs G., Vigeland S., Kramer M., Weisberg J. M., Lyne A. G., 2005, *MNRAS*, 364, 1397
Johnston S., Karastergiou A., 2017, *MNRAS*, 467, 3493
Johnston S., Kramer M., Karastergiou A., Hobbs G., Ord S., Wallman J., 2007, *MNRAS*, 381, 1625
Johnston S., Weisberg J. M., 2006, *MNRAS*, 368, 1856
Karastergiou A., Johnston S., 2004, *MNRAS*, 352, 689
Karastergiou A., Johnston S., 2007, *MNRAS*, 380, 1678
Keith M. J., Johnston S., Weltevrede P., Kramer M., 2010, *MNRAS*, 402, 745
Komesaroff M. M., 1970, *Nature*, 225, 612
Kramer M., Johnston S., 2008, *MNRAS*, 390, 87
Kramer M., Xilouris K. M., Lorimer D. R., Doroshenko O., Jessner A., Wielebinski R., Wolszczan A., Camilo F., 1998, *ApJ*, 501, 270
Luo Q., Melrose D. B., 2001, *MNRAS*, 325, 187
Lyne A. G., Manchester R. N., 1988, *MNRAS*, 234, 477
Lyne A. G., Smith F. G., 1968, *Nat*, 218, 124
Manchester R. N., Han J. L., Qiao G. J., 1998, *MNRAS*, 295, 280
Manchester R. N. et al., 2013, *PASA*, 30, e017
McKinnon M. M., Stinebring D. R., 1998, *ApJ*, 502, 883
Melrose D., Miller A., Karastergiou A., Luo Q., 2006, *MNRAS*, 365, 638
Melrose D. B., Luo Q., 2004, *MNRAS*, 352, 915

Mitra D., Basu R., Maciesiak K., Skrzypczak A., Melikidze G. I., Szary A., Krzeszowski K., 2016, *ApJ*, 833, 28
Mitra D., Rankin J. M., 2002, *ApJ*, 577, 322
Noutsos A., Johnston S., Kramer M., Karastergiou A., 2008, *MNRAS*, 386, 1881
Petrova S. A., 2006, *MNRAS*, 366, 1539
Petrova S. A., Lyubarskii Y. E., 2000, *A&A*, 355, 1168
Radhakrishnan V., Cooke D. J., 1969, *Ap. Lett.*, 3, 225
Radhakrishnan V., Rankin J. M., 1990, *ApJ*, 352, 258
Rankin J. M., 1990, *ApJ*, 352, 247
Rankin J. M., 1993, *ApJ*, 405, 285
Rookyard S. C., Weltevrede P., Johnston S., 2015a, *MNRAS*, 446, 3367
Rookyard S. C., Weltevrede P., Johnston S., 2015b, *MNRAS*, 446, 3356
Staveley-Smith L. et al., 1996, *PASA*, 13, 243
Tauris T. M., Manchester R. N., 1998, *MNRAS*, 298, 625
Thomas B. M., Greene K. J., James G. L., 1990, *I.E.E.E. Trans. Ant. Propag.*, 38, 1898
Tiburzi C. et al., 2013, *MNRAS*, 436, 3557
van Straten W., 2004, *ApJSS*, 152, 129
van Straten W., Manchester R. N., Johnston S., Reynolds J. E., 2010, *PASA*, 27, 104
van Straten W., Tiburzi C., 2017, *ApJ*, 835, 293
Weisberg J. M. et al., 1999, *ApJSS*, 121, 171
Weltevrede P., Johnston S., 2008, *MNRAS*, 391, 1210
Weltevrede P. et al., 2010, *PASA*, 27, 64

This paper has been typeset from a $\text{\TeX}/\text{\LaTeX}$ file prepared by the author.